Observation of lasing modes with exotic localized wave patterns from astigmatic large-Fresnel-number cavities

T. H. Lu,[2] Y. C. Lin,[1] H. C. Liang,[1] Y. J. Huang,[1] Y. F. Chen,[1,*] and K. F. Huang[1]

[1]*Department of Electrophysics, National Chiao Tung University, Hsinchu, Taiwan*
[2]*Department of Physics, National Taiwan Normal University, Taipei, Taiwan*
[*]*Corresponding author: yfchen@cc.nctu.edu.tw*

Received October 23, 2009; revised December 23, 2009; accepted December 28, 2009; posted January 7, 2010 (Doc. ID 118996); published January 26, 2010

We investigate the lasing modes in large-Fresnel-number laser systems with astigmatism effects. Experimental results reveal that numerous lasing modes are concentrated on exotic patterns corresponding to intriguing geometries. We theoretically use the quantum operator algebra to construct the wave representation for manifesting the origin of the localized wave patterns. © 2010 Optical Society of America

OCIS codes: 070.1675, 070.2580.

Laser resonators have been employed as analogous systems for generating high-order lasing modes to manifest the wave patterns of quantum coherent states, especially for mesoscopic and macroscopic regions [1–4]. Various laser systems are widely used to study optical pattern formation including, the Laguerre–Gaussian (LG) modes, Hermite–Gaussian (HG) modes, and the generalized coherent states that form a general family to comprise the HG and LG mode families as special cases [5,6]. Recently, we have employed a large-Fresnel-number laser system with an off-axis pumping scheme to visualize the coherent optical waves with localization related to the Lissajous and trochoidal curves [7,8]. This result signifies that exploring the transformation geometry of quantum coherent states plays a significant role in understanding the quantum-classical connection. More importantly, the investigation of high-order laser modes is useful for developing the idea for generating the coherent structured light that can carry orbital angular momentum or contain optical vortices for many applications [9,10].

In this Letter we experimentally performed a very large off-axis pumping for studying the lasing modes under the influence of considerable astigmatism. We observed that numerous lasing modes with exotic localized wave patterns correspond to the topological transformations. We used the quantum operator algebra to derive the generalized unitary operator for generating the eigenmodes for the spherical cavity subject to the astigmatism effects. With the generalized unitary operator and the quantum-classical connection, the geometries corresponding to the localized lasing patterns can be perfectly manifested.

The present laser cavity was composed of a spherical mirror and a large-aperture gain medium, as shown in Fig. 1. The gain medium was an a-cut 2.0 at. % $Nd:YVO_4$ crystal with a length of 2 mm and a cross section of 8×8 mm^2 to comply with the requirement of the extremely high transverse orders. The pump source was a 2 W, 809 nm fiber-coupled laser diode with a core diameter of 100 μm. A coupling lens was used to focus the pump beam to be approximately 25 μm in the laser crystal. The spherical mirror was a 10 mm radius-of-curvature concave mirror with antireflection coating at the pumping wavelength on the entrance face ($R<0.2\%$), high-reflection coating at lasing wavelength ($R>99.8\%$), and high-transmission coating at the pumping wavelength on the other surface ($T<95\%$). One planar surface of the laser crystal was coated for antireflection at the pumping and lasing wavelengths; the other surface was coated to be an output coupler with a reflectivity of 99%. To generate the high-order modes subject to considerable astigmatism, the pumping beam was focused into the crystal in the region with a large off-axis displacement along the c axis and a rather small displacement along the b axis. We experimentally find that more than 100 different laser modes related to distinct localized wave patterns can be generated at different degenerate cavities. In addition to Lissajous and trochoidal patterns [7,8] shown in Figs. 2(a) and 2(b), new findings of numerous lasing patterns corresponding to the topological transformations can be observed, as shown in Figs. 2(c)–2(e). These patterns propagate in the cavity with localization on 3D parametric surfaces, which is distinct from M mode and spiral beams. Since the laser cavity is an excellent analog system for studying the coherent waves, the understanding of these wave patterns should provide some useful insights into the fundamental behavior of wave functions at the border of the classical and quantum regimes.

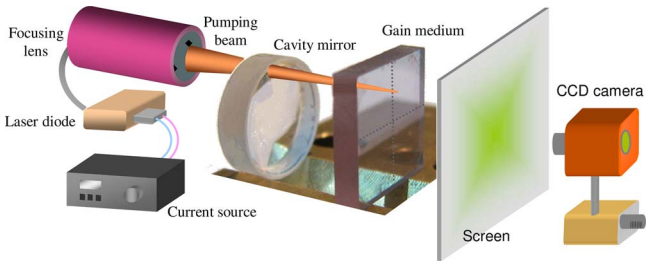

Fig. 1. (Color online) Experimental setup for the generation of high-order lasing modes in astigmatic cavities with an off-axis pumping scheme.

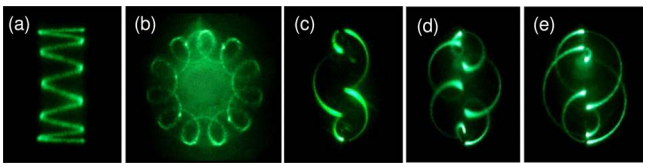

Fig. 2. (Color online) Experimental far-field patterns: (a) Lissajous pattern; (b) trochoidal pattern; (c), (d) other typical lasing patterns.

The paraxial eigenmodes of stable spherical cavities can be expressed as the normalized HG modes [11] $\Phi^{(\mathrm{HG})}_{m,n,l}(x,y,z)=\Phi^{(\mathrm{HG})}_{m,n}(x,y,z)e^{i(m+n+1)\theta_G(z)}e^{-i\zeta_{m,n,l}(x,y,z)}$, where

$$\Phi^{(\mathrm{HG})}_{m,n}(x,y,z)=\frac{1}{\sqrt{2^{m+n-1}\pi m!n!}}\frac{1}{w(z)}e^{-(x^2+y^2/w(z)^2)}\times H_m\left(\frac{\sqrt{2}}{w(z)}x\right)H_n\left(\frac{\sqrt{2}}{w(z)}y\right), \quad (1)$$

$w(z)=w_o\sqrt{1+(z/z_R)^2}$, $\zeta_{m,n,l}(x,y,z)=(\omega_{m,n,l}z/c)[1+(x^2+y^2)/2(z^2+z_R^2)]$, w_o is the beam waist, z_R is the Rayleigh range, $\omega_{m,n,l}$ is the resonance frequency, m and n are the transverse mode indices, l is the longitudinal mode index, and $\theta_G(z)=\tan^{-1}(z/z_R)$ is the Gouy phase. In the spherical cavity, $\omega_{m,n,l}$ is given by $\omega_{m,n,l}=[l\omega_L+(m+n+1)\omega_T)]$, where ω_L is the longitudinal mode spacing and ω_T is the transverse mode spacing. Since the paraxial wave equation can be exactly mapped on the time-dependent 2D quantum harmonic oscillator, the quantum operator algebra can be employed to explore the eigenmodes for the spherical cavity with the astigmatism effects [12,13]. The equivalent Hamiltonian for the HG modes can be expressed as $\hat{H}_o=\omega_T/2(\partial^2/\partial\tilde{x}^2+\partial^2/\partial\tilde{y}^2+\tilde{x}^2+\tilde{y}^2)$ with $\hat{H}_o|\Phi^{(\mathrm{HG})}_{m,n}\rangle=(m+n+1)\omega_T|\Phi^{(\mathrm{HG})}_{m,n}\rangle$, where $\tilde{x}=\sqrt{2}x/w$ and $\tilde{y}=\sqrt{2}y/w$ are dimensionless spatial variables. The operators for astigmatism and anisotropic effects can be expressed as $\hat{L}_1=\frac{1}{2}(\tilde{x}\tilde{y}+\partial/\partial\tilde{x}\partial/\partial\tilde{y})$, $\hat{L}_2=1/2i(\tilde{x}\partial/\partial\tilde{y}-\tilde{y}\partial/\partial\tilde{x})$, $\hat{L}_3=\frac{1}{4}(\tilde{x}^2+\partial^2/\partial\tilde{x}^2-\tilde{y}^2-\partial^2/\partial\tilde{y}^2)$ [12]. Without loss of generality, we model the 2D deformed harmonic oscillator as $\hat{H}_p=\hat{H}_0+A\cdot\hat{L}_1+B\cdot\hat{L}_2+C\cdot\hat{L}_3$ to consider the astigmatism and anisotropic effects, where A, B, and C are constants and usually significantly smaller than ω_T. The operators $\hat{L}_1$, $\hat{L}_2$ and $\hat{L}_3$ have been verified to satisfy the Lie commutator algebra $[\hat{L}_i,\hat{L}_j]=i\varepsilon_{i,j,k}\hat{L}_k$, where the Levi–Civita tensor $\varepsilon_{i,j,k}$ is equal to +1 and −1 for even and odd permutations of its indices, respectively, and zero otherwise [14]. With the SU(2) algebra, the eigenstates of $\hat{H}_p$ can be derived to be $|\Phi^{\alpha,\beta}_{m,n}\rangle=\hat{U}|\Phi^{(\mathrm{HG})}_{m,n}\rangle$ where $\hat{U}=e^{-i\alpha\hat{L}_3}e^{-i\beta\hat{L}_2}$, $\alpha=\tan^{-1}(B/A)$, and $\beta=\tan^{-1}(\sqrt{A^2+B^2}/C)$. This continuous transition between HG and LG modes is analogous to the transition between linear and circular polarization on the Poincaré sphere [15]. In terms of the Wigner d-matrix elements, the eigenstates $|\Phi^{\alpha,\beta}_{m,n}\rangle$ can be explicitly expressed as a linear combination of the states $|\Phi^{(\mathrm{HG})}_{m,n}\rangle$: $|\Phi^{\alpha,\beta}_{m,n}\rangle=\sum_{s=0}^{m+n}e^{-is\alpha}d^{m+n/2}_{s-m+n/2,m-n/2}(\beta)|\Phi^{(\mathrm{HG})}_{s,m+n-s}\rangle$, where

$$d^{m+n/2}_{s-(m+n)/2,m-n/2}(\beta)=\sqrt{s!(m+n-s)!m!n!}\sum_{\nu=\max[0,s-m]}^{\min[n,s]}\times\frac{(-1)^\nu(\cos(\beta/2))^{n+s-2\nu}(\sin(\beta/2))^{m-s+2\nu}}{\nu!(n-\nu)!(s-\nu)!(m-s+\nu)!}. \quad (2)$$

The state $|\Phi^{\alpha,\beta}_{m,n}\rangle$ for $\alpha=0$ can be viewed as a rotation of the HG mode $|\Phi^{(\mathrm{HG})}_{m,n}\rangle$ with an angle $\beta/2$ in the (x,y) plane [5]. Figures 3(a)–3(e) show the numerical wave patterns for the eigenstates $|\Phi^{\alpha,\beta}_{m,n}\rangle$ with $(m,n)=(18,55)$, $\alpha=\pi/2$ and five different β values. It can be seen that the states $|\Phi^{\alpha,\beta}_{m,n}\rangle$ for $\alpha=\pi/2$ with the parameter β changing from 0 to $\pi/2$ correspond to the astigmatic transformation from the HG mode to the LG mode [5,6].

Experimental results have evidenced that [7,8] that the longitudinal-transverse coupling in the large-Fresnel-number cavity usually forces the ratio ω_T/ω_L to be locked to a rational number P/Q. As a result, the group of the HG modes $\Phi^{(HG)}_{m_o+pk,n_o+qk,l_o+sk}$ with $k=0,1,2,3\cdots$ forms a family of frequency degenerate states, where the integers (p,q,s) obey the equation $s+(p+q)(P/Q)=0$. It has been verified [7] that the three-dimensional (3D) coherent states constructed by the family of $\Phi^{(\mathrm{HG})}_{m_o+pk,n_o+qk,l_o+sk}$ can be expressed as $|\Psi^{p,q,s}_{m_o,n_o,l_o}(\varphi)\rangle=\sum_{k=-M}^{M}C_{M,k}e^{ik\varphi}|\Phi^{(\mathrm{HG})}_{m_o+pk,n_o+qk,l_o+sk}\rangle$, where $C_{M,k}=2^{-M}\binom{2M}{M+k}^{1/2}$ is the weighting coefficient, $\binom{n}{k}=n!/k!(n-k)!$ represents the binomial coefficient, and the parameter φ is the relative phase between various HG modes at $z=0$. With the expression of Eq. (1), we can obtain $|\Psi^{p,q,s}_{m_o,n_o,l_o}(\varphi)\rangle=|\Psi^{p,q}_{m_o,n_o}(\varphi)\rangle e^{i(m_o+n_o+1)\theta_G(z)}e^{-i\zeta_{m_o,n_o,l_o}(x,y,z)}$ with $|\Psi^{p,q}_{m_o,n_o}(\varphi)\rangle=\sum_{k=-M}^{M}C_{M,k}e^{ik\phi(z)}e^{ik\varphi}|\Phi^{(\mathrm{HG})}_{m_o+pk,n_o+qk}\rangle$, where $\phi(z)=(p+q)\theta_G(z)$. Here, m_0 and n_0 indicate the order of the coherent state; M, the number of eigenstates involved in the superposition, is much smaller than m_0 and n_0. As discussed earlier, the astigmatism and anisotropic effects can be considered with the unitary operator $\hat{U}=e^{-i\alpha\hat{L}_3}e^{-i\beta\hat{L}_2}$. Consequently, the 3D coherent states subject to the astigmatism effect can be given by $\hat{U}|\Psi^{p,q,s}_{m_o,n_o,l_o}(\varphi)\rangle$, and their wave patterns are determined by the wave function $\hat{U}|\Psi^{p,q}_{m_o,n_o}(\varphi)\rangle=\sum_{k=-M}^{M}C_{M,k}e^{ik\phi(z)}e^{ik\varphi}|\Phi^{\alpha,\beta}_{m_o+pk,n_o+qk}\rangle$. The state $|\Psi^{p,q}_{n_o,m_o}(\varphi)\rangle$ has been verified to have the intensity lo-

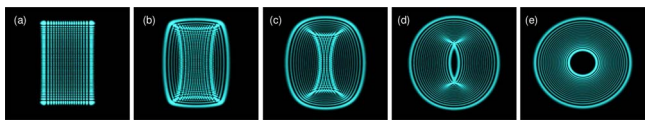

Fig. 3. (Color online) Numerical wave patterns for the intensity of eigenstates $|\Phi^{\alpha,\beta}_{m,n}\rangle$ with $(m,n)=(18,55)$, $\alpha=\pi/2$: (a) $\beta=0$, (b) $\beta=\pi/8$, (c) $\beta=\pi/4$, (d) $\beta=3\pi/8$, (e) $\beta=\pi/2$.

calized on the Lissajous parametric surface: $x=\mathrm{Re}[X(\vartheta,z)]$; $y=\mathrm{Re}[Y(\vartheta,z)]$, where $0\leqslant\vartheta\leqslant 2\pi$, $-\infty\leqslant z\leqslant\infty$, $X(\vartheta,z)=\sqrt{n_o}w(z)e^{i[q\vartheta+(\phi(z)+\varphi/p)]}$, and $Y(\vartheta,z)=\sqrt{m_o}w(z)e^{ip\vartheta}$ [7]. Using the isomorphic relation between SU(2) algebra and SO(3) algebra, the 3D coherent state $\hat{U}|\Psi^{p,q}_{m_o,n_o}(\varphi)\rangle$ can be deduced to be localized on the parametric surface: $x=\mathrm{Re}[\tilde{X}(\vartheta,z)]$; $y=\mathrm{Re}[\tilde{Y}(\vartheta,z)]$, where

$$\begin{bmatrix}\tilde{X}(\vartheta,z)\\ \tilde{Y}(\vartheta,z)\end{bmatrix}=\begin{bmatrix}e^{-i\alpha/2}\cos\left(\frac{\beta}{2}\right) & -e^{-i\alpha/2}\sin\left(\frac{\beta}{2}\right)\\ e^{i\alpha/2}\sin\left(\frac{\beta}{2}\right) & e^{i\alpha/2}\cos\left(\frac{\beta}{2}\right)\end{bmatrix}\times\begin{bmatrix}X(\vartheta,z)\\ Y(\vartheta,z)\end{bmatrix}. \quad (3)$$

Figures 4(a)–4(e) show the classical periodic orbits computed with the parametric curves in Eq. (3) to characterize the lasing patterns shown in Figs. 2(a)–2(e). The parameters are deduced from the best fit to the experimental patterns; where $(p,q)=(-1,10)$, $(m_o,n_o)=(40,200)$, $(\alpha,\beta)=(0,0)$ for Fig. 4(a); $(p,q)=(-1,10)$, $(m_o,n_o)=(50,500)$, $(\alpha,\beta)=(\pi/2,\pi/2)$ for Fig. 4(b); $(p,q)=(1,4)$, $(m_o,n_o)=(80,500)$, $(\alpha,\beta)=(\pi/2,\pi/3)$ for Fig. 4(c); $(p,q)=(1,6)$, $(m_o,n_o)=(80,500)$, $(\alpha,\beta)=(\pi/2,\pi/3)$ for Fig. 4(d); $(p,q)=(2,5)$, $(m_o,n_o)=(100,400)$, $(\alpha,\beta)=(\pi/2,\pi/3)$ for Fig. 4(e). The good agreement validates our quantum operator model and confirms the representation of the 3D coherent states $\hat{U}|\Psi^{p,q}_{m_o,n_o}(\varphi)\rangle$.

Finally, it is worth while mentioning that the transverse patterns of all experimental modes are position dependent during propagation. Figure 5(a) shows the variation of the experimental transverse patterns during propagation for the case corresponding to the far-field pattern in Fig. 2(c). We also use the 3D coherent state $\hat{U}|\Psi^{p,q}_{m_o,n_o}(\varphi)\rangle$ to mimic the experimental wave pattern [Fig. 5(b)] corresponding to Fig. 2(c) and to manifest the phase distribution for a small region, as shown in Fig. 5(c).

In summary, we have experimentally observed numerous lasing modes with exotic localized wave patterns from spherical cavities subject to considerable astigmatism. We have employed the quantum operator algebra to model the wave equation with the astigmatism effects and have derived a generalized unitary operator to obtain the eigenmodes. With the generalized unitary operator and the quantum-classical connection, we have perfectly manifested the geometries corresponding to the localized lasing patterns.

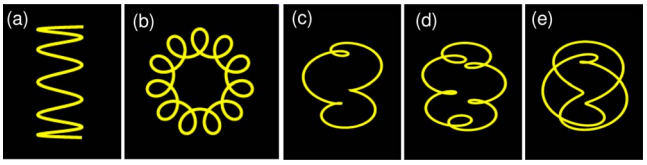

Fig. 4. (Color online) (a)–(e) Geometric curves with Eq. (3) corresponding to the experimental wave patterns shown in Fig. 1. Detailed description for the parameters; see text.

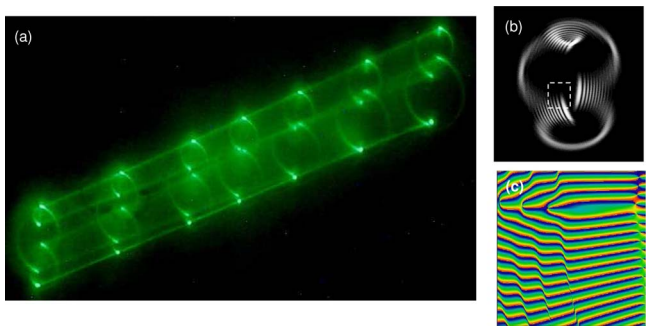

Fig. 5. (Color online) (a) Propagation-dependent experimental patterns of Fig. 2(a) from beam waist to 0.33 z_R; (b) numerical wave patterns corresponding to the experimental wave patterns shown in Fig. 2(c) with $(p,q)=(1,4)$, $(m_0,n_0)=(10,60)$; (c) phase distribution of the boxed region shown in (b).

This work is supported by the National Science Council of Taiwan (NSCT) (contract NSC-94-2112-M-009-034).

References

1. M. Brambilla, F. Battipede, L. A. Lugiato, V. Penna, F. Prati, C. Tamm, and C. O. Weiss, Phys. Rev. A **43**, 5090 (1991).
2. D. Dangoisse, D. Hennequin, C. Lepers, E. Louvergneaux, and P. Glorieux, Phys. Rev. A **46**, 5955 (1992).
3. E. Cabrera, O. G. Calderón, S. Melle, and J. M. Guerra, Phys. Rev. A **73**, 053820 (2006).
4. K. F. Huang, Y. F. Chen, H. C. Lai, and Y. P. Lan, Phys. Rev. Lett. **89**, 224102 (2002).
5. E. G. Abramochkin and V. G. Volostnikov, J. Opt. A **6**, S157 (2004).
6. L. E. Vicent and K. B. Wolf, J. Opt. Soc. Am. A **25**, 1875 (2008).
7. Y. F. Chen, T. H. Lu, K. W. Su, and K. F. Huang, Phys. Rev. Lett. **96**, 213902 (2006).
8. T. H. Lu, Y. C. Lin, Y. F. Chen, and K. F. Huang, Phys. Rev. Lett. **101**, 233901 (2008).
9. M. S. Soskin, V. N. Gorshkov, M. V. Vasnetsov, J. T. Malos, and N. R. Heckenberg, Phys. Rev. A **56**, 4064 (1997).
10. S. J. Van Enk and G. Nienhuis, J. Mod. Opt. **41**, 963 (1994).
11. G. Nienhuis and L. Allen, Phys. Rev. A **48**, 656 (1993).
12. S. J. van Enk and G. Nienhuis, Opt. Commun. **94**, 147 (1992).
13. G. Nienhuis and J. Visser, J. Opt. A **6**, 248 (2004).
14. J. Schwinger, in *Quantum Theory of Angular Momentum*, L. C. Biedenharn and H. van Dam, eds. (Academic, 1965), pp. 229–279.
15. J. Visser and G. Nienhuis, Phys. Rev. A **70**, 013809 (2004).